ChemComm

COMMUNICATION

View Article Online
View Journal | View Issue

Cite this: *Chem. Commun.*, 2026, **62**, 9904

Received 4th March 2026,
Accepted 20th April 2026

DOI: 10.1039/d6cc01319h

rsc.li/chemcomm

Unlocking efficient near-infrared circularly polarized phosphorescence reaching 800 nm in cyclometalated Pt(II) complexes

Shilin Gu,[a] Dongsheng Li,[a] Deng Long,[a] Xinglin Yu,[a] Wentao Li,*[a] Sihan Ma*[a] and Peng Tao*[b]

We report a promising strategy to design efficient NIR chiral Pt(II) complexes *via* ligand regulation and planar chirality formation, affording binuclear Pt(II) enantiomers that exhibit unprecedented NIR CPP reaching 800 nm, photoluminescence quantum yields of up to 35.4%, and luminescence dissymmetry factors of ~3.9 × 10^{-3}.

Near-infrared (NIR) circularly polarized (CP) luminescent (CPL) materials are promising for use in both biomedical engineering and optoelectronics.[1] Traditional methods of generating CP light *via* polarizers are energy-intensive.[1] Developing chiral luminescent materials that directly emit NIR CPL light is crucial. Integrating chirality into high-efficiency NIR emitters is therefore key to creating direct NIR CPL light sources with minimal energy loss. Phosphorescent transition-metal complexes (PTMCs) are particularly attractive because strong spin–orbit coupling (SOC) enables full utilization of both singlet and triplet excitons,[2] resulting in near-unity internal quantum efficiency.[3] Among PTMCs, Pt(II) complexes are promising candidates owing to the easy realization of long-wavelength emission.[2,3] However, the traditional HC^N ligand-based Pt(II) complexes usually suffer from low photoluminescence (PL) quantum yields (PLQYs) in the NIR region due to the lack of strong intermolecular interactions, leading to inefficient intersystem crossing (ISC) from the singlet excited state (S_1) to the triplet excited state (T_1).[4] Achieving Pt(II) complexes with high-efficiency near-infrared circularly polarized phosphorescence (CPP) remains a formidable challenge.[1]

The Pt–Pt interactions could promote the overlap of metal-centred orbitals, resulting in the formation of a low-energy triplet metal–metal-to-ligand charge transfer (^{3}MMLCT) state, which typically serves as an energy trap.[3c,5] The enhanced metal character strengthens SOC, facilitating both ISC from S_1 to T_1 and formally forbidden triplet-to-singlet radiative transition, thereby increasing the radiative decay rate.[5] Meanwhile, the ordered molecular alignment induced by Pt–Pt interactions restricts ligand vibrations and rotations, effectively suppressing non-radiative decay pathways linked to molecular motion and significantly lowering the non-radiative decay rate.[5] Thus, engineering Pt–Pt interactions offers a promising strategy to reduce non-radiative loss in low-energy NIR Pt(II) emitters by enhancing the radiative decay rate constant and ultimately improving their PLQYs. Furthermore, although Pt(II) complexes can be endowed with CPP upon the introduction of helical or point chirality,[6] intramolecular Pt–Pt interactions could also provide an opportunity to generate planar chirality for realizing circularly polarized phosphorescence of Pt(II) complexes.[5]

In this communication, a promising strategy was proposed to design highly efficient NIR chiral Pt(II) complexes ((***R*,*S*,*R***)-**Pt1**, (***S*,*R*,*S***)-**Pt1**, (***R*,*S*,*R***)-**Pt2**, and (***S*,*R*,*S***)-**Pt2**) *via* rational ligand regulation and planar chirality formation (Scheme 1). Two isoquinoline derivatives (*i.e.*, 1-(4-fluorophenyl)isoquinoline and 1-(benzo[*b*]thiophen-2-yl)isoquinoline-4-carbonitrile) with low triplet energy levels were selected as the cyclometalating ligands. The point chirality of the bridging ligand enables exceptional diastereoselectivity promoted by the intramolecular Pt–Pt interaction, affording pure binuclear Pt(II) enantiomers that exhibit unprecedented NIR CPP reaching 800 nm, notable PLQYs of up to 35.4%, short excited state lifetimes within 2 μs, and appreciable luminescence dissymmetry factors (g_{lum}) of up to ~3.9 × 10^{-3}. To the best of our knowledge, this is the first example of highly efficient NIR chiral binuclear Pt(II) complexes with CPP maxima reaching 800 nm.[1]

The target Pt(II) complexes were obtained as deep red or dark maroon solids by heating a chiral bridging ligand with the Pt(II) intermediate [Pt(F-piq)(F-Hpiq)Cl] or [Pt(CN-iqbt)(CN-Hiqbt)Cl] in the presence of K_2CO_3 at 80 °C in a sealed tube with CH_2Cl_2 under an argon atmosphere (Scheme S1). Notably, in all coordination reactions, only one enantiomerically pure product

---

[a] *Institute of Advanced Optoelectronic Materials and Technology, College of Big Data and Information Engineering, Guizhou University, Guiyang 550025, P. R. China. E-mail: wtli@gzu.edu.cn, shma@gzu.edu.cn*
[b] *Department of Applied Biology and Chemical Technology, The Hong Kong Polytechnic University, Hung Hom, Hong Kong, P. R. China. E-mail: pengtao@polyu.edu.hk*

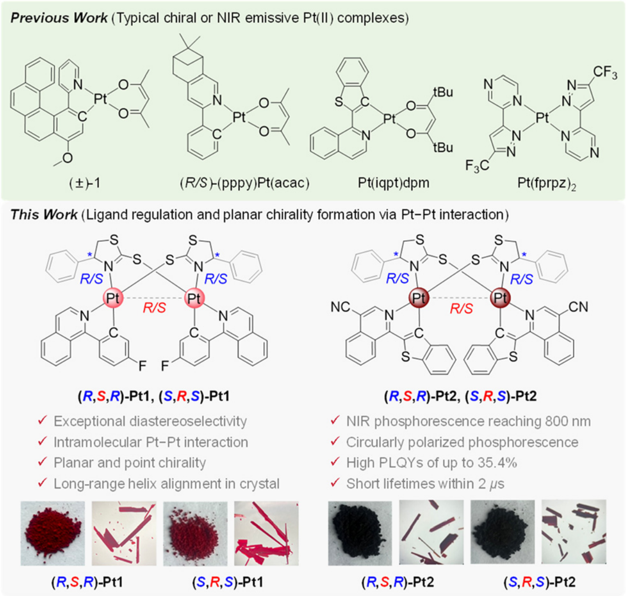

Scheme 1 Molecular engineering of cyclometalated Pt(II) complexes showing highly efficient NIR CPP reaching 800 nm in this work and the typical examples of the reported chiral or NIR emissive Pt(II) complexes. Insets show the photographs of these complexes in powder (left) and crystal (right) states under room light.

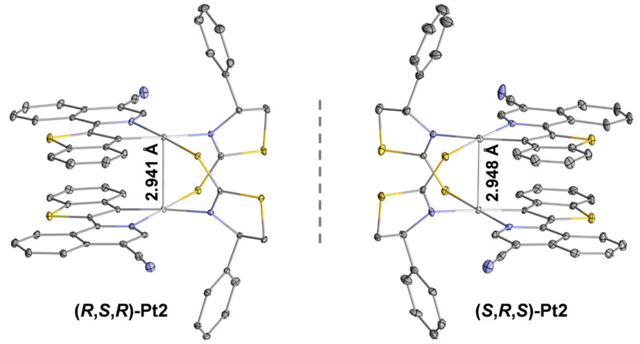

Fig. 1 Crystal structures of **(*R*,*S*,*R*)/(*S*,*R*,*S*)-Pt2** showing the distance of the intramolecular Pt–Pt interactions. Note: the carbon atoms are shown in gray, nitrogen atoms in light blue, platinum atoms in light gray, and sulfur atoms in yellow.

could be isolated, indicating nearly perfect diastereoselectivity (close to 100%). This high selectivity is likely driven by the point chirality of the chiral bridging ligand, which is in good agreement with previously reported observations.[5b,c] These Pt(II) enantiomers were well characterized by nuclear magnetic resonance (NMR) spectroscopy, elemental analysis, and mass spectrometry (MS). ^{1}H, ^{13}C{^{1}H}, and ^{19}F{^{1}H} NMR spectra all exhibit distinct and well-resolved resonance signals. The typical chemical shifts of the ^{1}H, ^{13}C, and ^{19}F nuclei are provided in Table S1. For each pair of enantiomers, identical NMR spectra are observed in $CDCl_3$, which is attributed to their identical atomic connectivity and equivalent electronic environments surrounding the nuclei. Only one ^{19}F resonance signal (~ -110.87 ppm) was observed for **(*R*,*S*,*R*)-Pt1** and **(*S*,*R*,*S*)-Pt1**, implying the presence of molecular symmetry in binuclear complexes.

The Pt(II) enantiomers were unambiguously confirmed by single-crystal X-ray diffraction analysis (Table S2). The crystallographic data revealed that the Pt(II) centres adopt a slightly distorted square-planar geometry. In this configuration, the nitrogen atoms from both the cyclometalated and bridging ligands are coordinated in a *trans* arrangement, while the metalated carbon and the sulfur atom from the adjacent bridging ligand are coordinated in a *cis* manner, which aligns with previously reported complexes.[5,7] The bond distances for Pt–C, Pt–N, and Pt–S fall within the ranges of 1.98–2.02 Å, 2.04–2.15 Å, and 2.28–2.30 Å, respectively (Table S3). Notably, the Pt–N bond lengths vary considerably depending on the N-donor strength of the ligands, with a significantly elongated Pt–N bond observed for the bridging ligand. Furthermore, the C–Pt–N bond angles are ~80° (Table S3), indicating a minor deviation from ideal square-planar geometry, which can be attributed to the Jahn–Teller effect.[5,7] As shown in Fig. 1 and Fig. S1, short intramolecular Pt–Pt distances were observed, measuring 2.922 and 2.910 Å for **(*R*,*S*,*R*)/(*S*,*R*,*S*)-Pt1** enantiomers, and 2.941 and 2.948 Å for the **(*R*,*S*,*R*)/(*S*,*R*,*S*)-Pt2** pair. The slightly longer Pt–Pt distances in the **Pt2** complexes compared to those in the **Pt1** pair suggest that the intramolecular Pt–Pt interactions can be modulated by the choice of cyclometalating ligands. The two cyclometalated ligands are oriented in a head-to-tail manner. In all crystal structures, intermolecular face-to-face π–π stacking interactions with distances ranging from 3.37 to 3.42 Å are observed between partially overlapping cyclometalated ligands of adjacent molecules (Fig. S1, S2 and Table S4). Additionally, various weak intermolecular contacts including S⋯H and F⋯H interactions with distances below 3 Å are present throughout the crystals, contributing to the formation of a long-range helical arrangement (Fig. S3 and Table S4).

To explore the optical properties of Pt(II) complexes, their ultraviolet (UV)–visible (vis) absorption spectra were measured in CH_2Cl_2 at 1.0×10^{-5} M at ambient temperature. As depicted in Fig. 2a, the complexes exhibit typical absorption profiles. An intense absorption band observed in the high-energy region (240–380 nm) originates from the $\pi \rightarrow \pi^*$ transitions of the ligands.[5] Conversely, the weaker and lower-energy absorption band spanning 380–700 nm is associated with MMLCT transitions (Table S5).[5] To gain deeper insight into the electronic transition characteristics, time-dependent density functional theory (TD-DFT) calculations were performed.[8] The simulated absorption profiles of the complexes in CH_2Cl_2 are in good agreement with the experimental spectra (Fig. S4). The optimized S_0 and T_1 geometries of the complexes and their Pt–Pt distances are shown in Fig. S5. For all Pt(II) complexes, the low-energy absorption bands predominantly arise from the transition between the highest occupied molecular orbital (HOMO) and the lowest unoccupied molecular orbital (LUMO), with a contribution exceeding 99% (Table S6). As depicted in Fig. 3, the HOMO electron density is mainly localized on the two Pt centres, whereas the LUMO is largely distributed across the cyclometalated ligands. This distribution further corroborates the assignment of the low-energy absorption to MMLCT transitions. As listed in

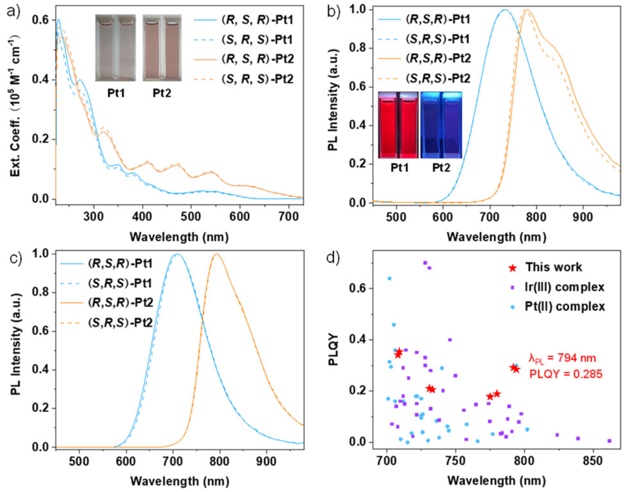

Fig. 2 UV-vis absorption spectra (a) and PL spectra (b) of Pt(II) complexes in degassed CH_2Cl_2; PL spectra (c) of Pt(II) complexes in a 5 wt% PMMA film at room temperature; (d) comparison of the PLQYs of the designed Pt(II) complexes with the reported complexes showing PL in the NIR region. Ext. Coeff. refers to the extinction coefficient.

Table S7, the Pt d_π orbital contributions to the HOMO and LUMO are 78.97% and 6.18% for ***(R,S,R)*-Pt1**, 79.10% and 6.00% for ***(S,R,S)*-Pt1**, 73.77% and 7.27% for ***(R,S,R)*-Pt2**, and 75.69% and 7.02% for ***(S,R,S)*-Pt2**, respectively. Meanwhile, the contributions from the π orbitals of the cyclometalated ligands to the HOMO and LUMO are 11.70% and 92.00% for ***(R,S,R)*-Pt1**, 11.39% and 92.25% for ***(S,R,S)*-Pt1**, 17.05% and 90.77% for ***(R,S,R)*-Pt2**, and 14.99% and 91.17% for ***(S,R,S)*-Pt2**, respectively. The TD-DFT-calculated HOMO–LUMO energy gaps are 2.99 and 2.94 eV for the **Pt1** enantiomers, and 2.71 and 2.67 eV for the **Pt2** pair.

Upon UV light excitation, all Pt(II) enantiomers exhibit intense NIR phosphorescence both in degassed CH_2Cl_2 and in poly(methyl methacrylate) (PMMA) films doped at 5 wt% under ambient conditions. As depicted in Fig. 2b and c, the **Pt1** enantiomers show emission maxima at approximately 733 nm in degassed CH_2Cl_2 and around 709 nm in the PMMA matrix. In contrast, the **Pt2** pair displays significantly red-shifted phosphorescence reaching 800 nm in both media, implying that the emission originates from individual molecules and the emission energies could be further decreased by lowering the triplet energy levels of cyclometalated ligands in the binuclear Pt(II) systems featuring strong intramolecular Pt–Pt interactions. Notably, the PLQYs of these complexes increase substantially upon dispersion in the rigid PMMA matrix, increasing from 0.178–0.21 in degassed CH_2Cl_2 to 0.285–0.354 in the doped films (Table S5). This enhancement indicates that non-radiative decay pathways are effectively suppressed in the rigid environment. Fig. 2d depicts the comparison of the PLQYs of the designed Pt(II) complexes in this work with those of the reported Ir(III) and Pt(II) complexes showing PL in the NIR region, highlighting the effectiveness of the molecular design strategy employed in this work. The emission is further characterized by large Stokes shifts and long-lived excited states with lifetimes ranging from 0.32 to 0.40 μs in degassed CH_2Cl_2 and from 1.25 to 1.84 μs in PMMA films (Fig. S6 and Table S5). These features are consistent with phosphorescence originating from triplet excited states.[5] The observed long-wavelength NIR phosphorescence at room temperature can be ascribed to the intrinsically low triplet energy levels of the cyclometalated ligands, combined with the formation of triplet ^{3}MMLCT states facilitated by strong intramolecular Pt–Pt and π–π interactions.

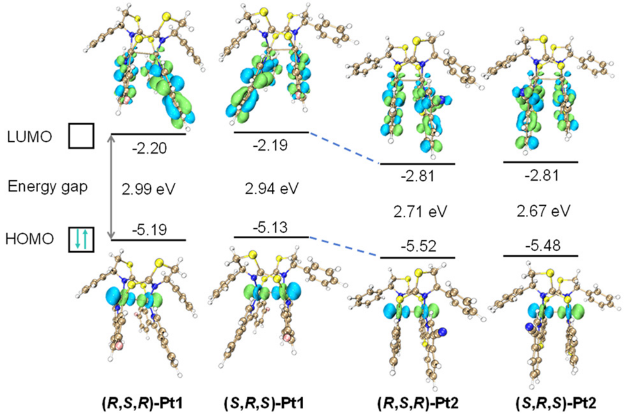

Fig. 3 Calculated electron cloud distributions and the orbital energy levels of the LUMO and HOMO for Pt(II) complexes at their geometrical optimized ground state.

The electrochemical behaviour of the Pt(II) complexes was investigated by cyclic voltammetry in CH_3CN (Fig. S7). Oxidation potentials centred on the Pt atoms were determined to be 0.61/0.60 eV for the **Pt1** enantiomers and 0.89/0.88 eV for the **Pt2** pair (Table S8). This assignment is supported by DFT calculations, which reveal that the HOMO is predominantly localized on the Pt centers (Pt dπ orbital contributions: 73.77–79.10%), with minimal ligand contribution. From the absorption edges, the HOMO and LUMO energy levels were calculated to be −4.90/−4.89 eV and −2.93/−2.92 eV for **Pt1** enantiomers, and −5.18/−5.17 eV and −3.58/−3.57 eV for the **Pt2** pair, respectively.

The chiroptical properties of the Pt(II) complexes were further evaluated in CH_2Cl_2 using circular dichroism (CD) and CPL spectroscopy. As shown in Fig. 4, mirror-image CD signals were observed for each enantiomeric pair as well as for the corresponding free chiral ligands. The experimental CD spectra closely matched the simulated results (Fig. S8 and Tables S9, S10), further confirming the absolute configurations. Based on TD-DFT calculations, the CD bands in the 470–700 nm region primarily arise from planar chirality.[7] CPL spectra were acquired both in CH_2Cl_2 solution and in PMMA films. Mirror-image CPL responses were clearly observed for each pair of enantiomers (Fig. 4c and e). The g_{lum} values at the emission maxima were determined to be $-2.5/2.5 \times 10^{-3}$ in CH_2Cl_2 and $-2.8/2.7 \times 10^{-3}$ in PMMA for ***(R,S,R)*/*(S,R,S)*-Pt1**, and $-2.1/2.1 \times 10^{-3}$ in CH_2Cl_2 and $-3.9/3.8 \times 10^{-3}$ in PMMA for ***(R,S,R)*/*(S,R,S)*-Pt2** (Table S5, Fig. 4 and Fig. S9). As far as we know, this is the first example of NIR chiral binuclear Pt(II) complexes with CPP maxima reaching 800 nm.[1] For compounds with small molecular weight, g_{lum} is given by $g_{\text{lum}} = 4\cos\theta|\boldsymbol{\mu}_e||\boldsymbol{\mu}_m|/(|\boldsymbol{\mu}_e|^2 + |\boldsymbol{\mu}_m|^2)$, where $\boldsymbol{\mu}_e$ and $\boldsymbol{\mu}_m$ are

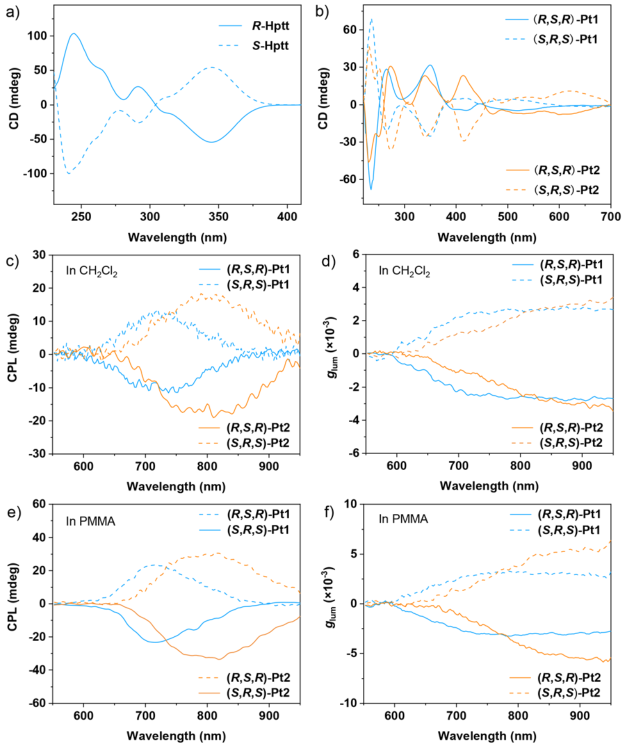

Fig. 4 CD spectra of free bridging ligands (a) and Pt(II) complexes (b) in CH_2Cl_2; the CPL (c) and (e) and g_{lum} profiles (d) and (f) of Pt(II) complexes in degassed CH_2Cl_2 and the PMMA film at room temperature.

the electric and magnetic transition dipole moments and θ is the angle between them.[1] The calculated $|\boldsymbol{\mu}_e|/|\boldsymbol{\mu}_m|$ values ($\times 10^{-20}$) are 3.9/0.006 for ***(R,S,R)*-Pt1**, 3.9/0.007 for ***(S,R,S)*-Pt1**, 2.9/0.002 for ***(R,S,R)*-Pt2**, and 3.0/0.002 for ***(S,R,S)*-Pt2** (Table S10). The corresponding θ values are 45.4°, 44.2°, 2.4°, and 0.4°, respectively. Notably, the molecular structure exerts a much stronger influence on $|\boldsymbol{\mu}_m|$ and θ than on $|\boldsymbol{\mu}_e|$. As expected, $|\boldsymbol{\mu}_e|$ is substantially larger than $|\boldsymbol{\mu}_m|$ for all complexes. The simulated g_{lum} values (3.3×10^{-3} for ***(R,S,R)*-Pt1**, -3.4×10^{-3} for ***(S,R,S)*-Pt1**, 1.8×10^{-3} for ***(R,S,R)*-Pt2**, and -1.6×10^{-3} for ***(S,R,S)*-Pt2**) are on the order of 10^{-3}, consistent with typical values of reported analogues.[1,9]

To conclude, we have developed a series of chiral binuclear Pt(II) complexes achieving NIR CPP up to 800 nm through rational ligand regulation and planar chirality engineering. The intramolecular Pt–Pt interactions not only promote the formation of ^{3}MMLCT states but also facilitate planar chirality. These complexes exhibit notable PLQYs (up to 35.4%), short lifetimes (<2 μs), and appreciable g_{lum} factors ($\sim 3.9 \times 10^{-3}$), representing the first example of NIR CPL Pt(II) emitters reaching 800 nm. These results demonstrate that this design strategy shows great potential for developing high-performance NIR CPL emitters for both biomedical and optoelectronic applications.

Conflicts of interest

There are no conflicts to declare.

Data availability

The data supporting this article have been included as part of the supplementary information (SI). Supplementary information: synthesis, characterization and other data. See DOI: https://doi.org/10.1039/d6cc01319h.

CCDC 2526096–2526099 contain the supplementary crystallographic data for this paper.[10a–d]

Acknowledgements

We acknowledge the financial support from the Guizhou University Talent Program (X2023159), the Guizhou Provincial Basic Research Program (Natural Science) (QKHJC MS[2025]606), the Guizhou Provincial Basic Research Program (Natural Science-Youth Guidance) (QKHJC2024Y100), the Youth Talent Growth Project of Guizhou Provincial Department of Education (QJJ2024023), the Guangdong Basic and Applied Basic Research Foundation (2026A1515011199), and the Startup Fund for RAPs under the Strategic Hiring Scheme (P0035922).

References

1 (*a*) N. Liang, C. Cao, Z. Xie, J. Liu, Y. Feng and C.-J. Yao, *Mater. Today*, 2024, **75**, 309; (*b*) X. Yang, X. Gao, Y.-X. Zheng, H. Kuang, C.-F. Chen, M. Liu, P. Duan and Z. Tang, *CCS Chem.*, 2023, **5**, 2760.
2 (*a*) K. Y. Zhang, Q. Yu, H. Wei, S. Liu, Q. Zhao and W. Huang, *Chem. Rev.*, 2018, **118**, 1770; (*b*) P. Tao, X. Lü, G. Zhou and W.-Y. Wong, *Acc. Mater. Res.*, 2022, **3**, 830; (*c*) P. Tao and W.-Y. Wong, Luminescent Transition-Metal Complexes and Their Applications in Electroluminescence, *Comprehensive Inorganic Chemistry III*, Elsevier, 3rd edn, 2023, vol. 8, pp. 2–79; (*d*) S. Hattori and K. Shinozaki, *ChemPhotoChem*, 2025, **9**, e202500041.
3 (*a*) P. Tao, J. Jin, X. Zheng, Y.-J. Pu and W.-Y. Wong, *Matter*, 2025, **8**, 102142; (*b*) S. N. T. Phan, N. B. Nguyen and T. S. Teets, *Chem. Commun.*, 2025, **61**, 17544; (*c*) K. T. Ly, R.-W. Chen-Cheng, H.-W. Lin, Y.-J. Shiau, S.-H. Liu, P.-T. Chou, C.-S. Tsao, Y.-C. Huang and Y. Chi, *Nat. Photonics*, 2017, **11**, 63; (*d*) M. Wałęsa-Chorab, *J. Photochem. Photobiol., C*, 2024, **59**, 100664; (*e*) H. J. Park, *Crystals*, 2025, **15**, 273.
4 M. Penconi, M. Cazzaniga, S. Kesarkar, P. R. Mussini, D. Ceresoli and A. Bossi, *Photochem. Photobiol. Sci.*, 2017, **16**, 1220.
5 (*a*) M. Yoshida and M. Kato, *Coord. Chem. Rev.*, 2018, **355**, 101; (*b*) J. Song, H. Xiao, B. Zhang, L. Qu, X. Zhou, P. Hu, Z.-X. Xu and H. Xiang, *Angew. Chem., Int. Ed.*, 2023, **62**, e202302011; (*c*) J. Song, H. Xiao, L. Fang, L. Qu, X. Zhou, Z.-X. Xu, C. Yang and H. Xiang, *J. Am. Chem. Soc.*, 2022, **144**, 2233.
6 (*a*) J. R. Brandt, X. Wang, Y. Yang, A. J. Campbell and M. J. Fuchter, *J. Am. Chem. Soc.*, 2016, **138**, 9743; (*b*) G.-Z. Lu, N. Su, Y. Li and Y.-X. Zheng, *J. Organomet. Chem.*, 2017, **842**, 39.
7 (*a*) B. Zhang, Q. Yang, B. Tu, W. Dong, X. Zhou, J. Song and H. Xiang, *Org. Lett.*, 2025, **27**, 6971; (*b*) S. Gu, D. Li, D. Long, X. Yu, S. Ma, W. Li, J. Liu, P. Tao and W.-Y. Wong, *Inorg. Chem.*, 2025, **64**, 22513.
8 M. J. Frisch, G. W. Trucks, H. B. Schlegel, G. E. Scuseria, M. A. Robb, J. R. Cheeseman, G. Scalmani, V. Barone, G. A. Petersson, H. Nakatsuji, X. Li, M. Caricato, A. V. Marenich, J. Bloino, B. G. Janesko, R. Gomperts, B. Mennucci, H. P. Hratchian, J. V. Ortiz, A. F. Izmaylov, J. L. Sonnenberg, D. Williams-Young, F. Ding, F. Lipparini, F. Egidi, J. Goings, B. Peng, A. Petrone, T. Henderson, D. Ranasinghe, V. G. Zakrzewski, J. Gao, N. Rega, G. Zheng, W. Liang, M. Hada, M. Ehara, K. Toyota, R. Fukuda, J. Hasegawa, M. Ishida, T. Nakajima, Y. Honda, O. Kitao, H. Nakai, T. Vreven, K. Throssell, J. A. Montgomery, J. E. Peralta, F. Ogliaro, M. J. Bearpark, J. J. Heyd, E. N. Brothers, K. N. Kudin, V. N. Staroverov, T. A. Keith, R. Kobayashi, J. Normand, K. Raghavachari, A. P. Rendell, J. C. Burant, S. S. Iyengar, J. Tomasi, M. Cossi, J. M. Millam, M. Klene, C. Adamo, R. Cammi, J. W. Ochterski, R. L. Martin, K. Morokuma, O. Farkas, J. B. Foresman and D. J. Fox, *Gaussian 16, Revision C.01*, Gaussian, Inc., Wallingford, CT, p. 201.

9 (*a*) J. Han, S. Guo, H. Lu, S. Liu, Q. Zhao and W. Huang, *Adv. Opt. Mater.*, 2018, **6**, 1800538; (*b*) H. Lu, L. Di Bari and L. Favereau, *Nat. Photonics*, 2025, **19**, 1041; (*c*) F. J. Coughlin, M. S. Westrol, K. D. Oyler, N. Byrne, C. Kraml, E. Zysman-Colman, M. S. Lowry and S. Bernhard, *Inorg. Chem.*, 2008, **47**, 2039; (*d*) Y. Deng, M. Wang, Y. Zhuang, S. Liu, W. Huang and Q. Zhao, *Light: Sci. Appl.*, 2021, **10**, 76.

10 (*a*) CCDC 2526096: Experimental Crystal Structure Determination, 2026, DOI: 10.5517/ccdc.csd.cc2qslz3; (*b*) CCDC 2526097: Experimental Crystal Structure Determination, 2026, DOI: 10.5517/ccdc.csd.cc2qsm05; (*c*) CCDC 2526098: Experimental Crystal Structure Determination, 2026, DOI: 10.5517/ccdc.csd.cc2qsm16; (*d*) CCDC 2526099: Experimental Crystal Structure Determination, 2026, DOI: 10.5517/ccdc.csd.cc2qsm27.